RESEARCH

Stability of inner dump slope under coal pillar support: case study in an open-pit coal mine

Guanghe Li[1] · Xiaoxu Yang[1] · Dong Wang[1] · Yanting Wang[1] · Xiangyu Yu[1]

Abstract
The stability of an inner dump slope was investigated under the effect of coal pillar support considering the development position of dumping. Based on the instability mechanism and load distribution characteristics of the supporting coal pillar, the three-dimensional mechanical effects of the supporting coal pillar are characterized. Using the two-dimensional equivalent principle and the residual thrust method, the stability of the inner dump slope was analyzed under the effect of pillar support at different dump development positions. The quantitative effects of various factors on the inner dump slope stability were revealed, and the coal pillar shape parameters were optimized through numerical simulations. The results indicate that the slope stability coefficient is linearly related to the top width and height of the coal pillar, slope angle, and base inclination angle, and has an exponential relation with the coal pillar strike length and slope height increment. There are quadratic and absolute value relations with the coal pillar outer and the inner bottom angle, respectively. The top width of the coal pillar in the inner dump of Shengli East No.2 open-pit coal mine should be at a level of +824 m, and the optimal top width and height are 15 and 36.7 m, respectively. The instability mechanism of the supporting and retaining coal pillar obtained by numerical simulations and the stability of the inner dump are in good agreement with the theoretical analysis. Our results provide a theoretical basis for the design, treatment, and safe implementation of similar open-pit mine slope engineering.

Keywords Inner dump · Supporting coal pillar · Slope stability · Numerical simulation · Morphological parameters

1 Introduction

The enhanced internal drainage of open-pit mines reduces the floor space of external drainage, decreases the stripping distance, and improves the efficiency of equipment operation. It is also the best measure for controlling the spontaneous combustion of coal, dust, and slope stability. However, once the inner dump slope has been formed, its stability directly affects the development of the open-pit coal mine stripping project and the safety of personnel and equipment. The inner dumps of some large-scale open-pit coal mines in China have experienced a certain degree of deformation or instability, which seriously threatens the safe production of open-pit coal mines. For example, in September 2014, the Huolinhe open-pit coal mine found that the inner dump was in a creeping state. Although the overall deformation

was relatively stable, a bottom heave with a height of about 1 m appeared near the coal seam floor, and extended 700 m along the north–south direction. A landslide with a volume of about 770,000 m³ occurred in February 2015, causing the +828 m horizontal dumping pan to move forward by 75 m, and the height of the bottom drum near the F4 fault to shift between 0 and 29 m (Tang et al. 2016). The inner dump in the Shenhua Baorixile open-pit coal mine began to settle in April 2009. In May of the same year, the deformation of the inner dump site +660 m horizontal dumping transportation platform accelerated, and a 2-h landslide occurred. The landslide area covered about 750 m from north to south and about 600 m from east to west. The sliding distance was 200 m and the volume of the sliding body was estimated at about 10 million cubic meters, causing serious damage to the drainage system of the blind ditch in the basement (Yang et al. 2018). The main controlling factors of the inner dump slope are the weak base and groundwater. As the base rock mass of such dumps is highly hydrophilic, it is difficult to quantify the effect of conventional draining and drainage measures (Lu et al. 2019). If a substrate treatment is

✉ Guanghe Li
 li_7118@126.com

1 College of Mining, Liaoning Technical University, Fuxin 123000, Liaoning, China

performed, the peeling cost will increase; additionally, when the weak substrate layer is thick, it is difficult to obtain an ideal treatment effect (Zhang and Wang 2015). Retaining coal pillars are an important means of improving the stability of the inner dump slope. For example, Ji (2013) analyzed the stability of the inner dump under three potential landslide modes, and analyzed the influence of the width of the coal pillar on the stability of the inner dump. Wang et al. (2019) examined the mechanical effects of supporting coal pillars and revealed the quantitative relationship between coal pillar morphological parameters and other factors and supporting effects. Previous studies have only considered the two-dimensional supporting effect of coal pillars and have not investigated the impact of the discharge load on the supporting effect of the coal pillar, resulting in the remaining coal pillar being too large. Therefore, there is an urgent need to find a new method for analyzing the stability of the inner dump slope under the pillar supporting effect that takes into account the development position of the dump, so as to realize the safe and economical operation of open-pit coal mines.
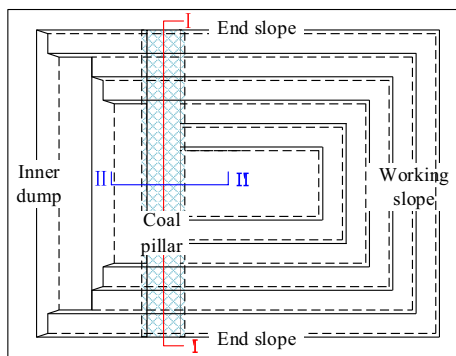

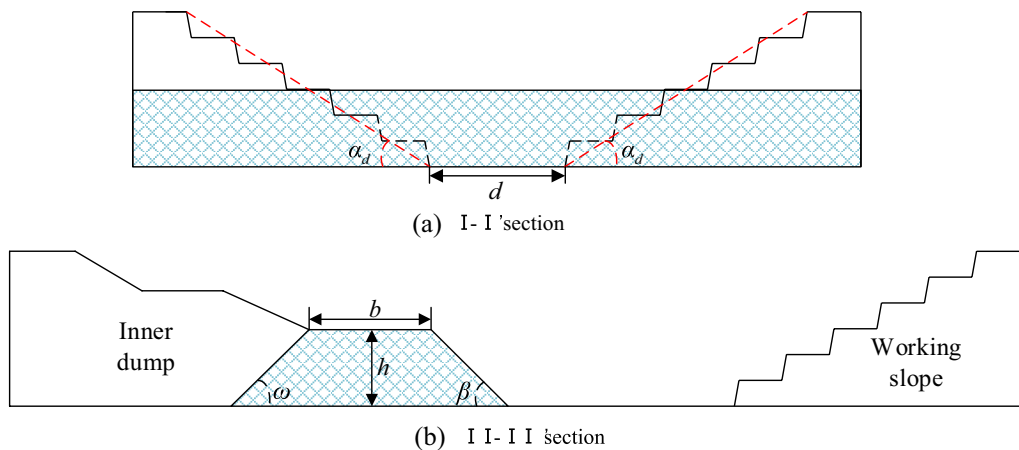**Fig. 1** Location of supporting coal pillar

2 Characterization of three-dimensional mechanical effects of supporting coal pillar

2.1 Analysis of instability mechanism of supporting coal pillarn

Given the current status of stripping projects in open-pit coal mines and the associated equipment operation requirements, the spatial form of the supporting coal pillar of the inner dump can be approximated as a hexahedron with a trapezoidal section. The plane position of the supporting coal pillar is shown in Fig. 1.

The shape of the section along the direction of the supporting coal pillar (I-I') is shown in Fig. 2a. The shape of the section along the inclination of the supporting coal pillar (II-II') is shown in Fig. 2b.

The sectional shape of the supporting coal pillar in the I-I' section can be regarded as an inverted trapezoid, and the sectional shape in the II-II' section can be regarded as a trapezoid. Assuming that the slope angle of the end slope is α_d, based on the positional relationship between the supporting coal pillar and the inner dump, the bottom angle of the trapezoid near the inner dump is the inner bottom angle ω of the supporting coal pillar, and the trapezoid near the goaf side of the bottom angle is the outside corner β of the supporting coal pillar. The height of the trapezoid is the height of the supporting coal pillar h, the top width of the trapezoid is the top width of the supporting coal pillar b, and the width of the open pit bottom is the strike length d of the supporting coal pillar.

The coal pillar is subjected to the static earth pressure F behind the inner dump, the squeezing force F_1 and F_2 of the side edges, the shear resistance T_1 and T_2 of the side interfaces, and the supporting force of the bottom interface
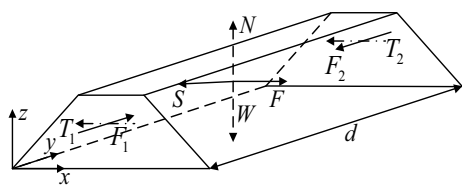

(a) I- I 'section

(b) I I- I I 'section

Fig. 2 Section shape of supporting coal pillar

Fig. 3 Spatial shape and force state of supporting coal pillar

Fig. 4 Failure position of supporting coal pillar

N. Under the effect of shear resistance *S* and gravity *W* (the resultant force of the weight of the coal pillar and the gravity load of the discharged material), the spatial shape and force analysis of the coal pillar are depicted in Fig. 3.

Although the supporting coal pillar is subjected to three-dimensional mechanics, it can be approximated using rock beam theory for analysis. It is well known that the supporting coal pillar is prone to shear failure on both sides of the end slope, and cracking damage can easily occur in the middle of the supporting coal pillar. When the supporting coal pillar is first broken by the static earth pressure *F* behind the inner dump, it can be roughly approximated as two cantilever beams. If the overall instability of the inner dump is induced, the two cantilever beams on either side of the end slope will undergo shear failure. In this study, the failure mechanism of the supporting coal pillar is similar to the shear failure of the lowermost rock strata in the inner row of the cross-mining in the Zhundong open-pit mine (Tian 2019). According to a large number of landslide engineering examples (Wang et al. 2020; Liu et al. 2020; Wei and Nei 2013), shear failure occurred in the lower rock mass and tensile fracture failure occurred in the upper rock mass, which eventually induced a landslide. Therefore, when the failure of the supporting coal pillar induces the overall instability of the slope, shear failure occurs near the end edge positions on both sides of the supporting coal pillar.

When the supporting coal pillar undergoes shear failure on both sides of the end slope, the resultant force must be greater than the shear resistance of the supporting coal pillar.
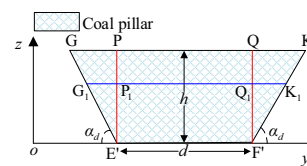
The position at which the resultant shear force *T* is the least likely to undergo shear failure can be determined as follows. Assuming that the shape of the side interface of the supporting coal pillar is the same and the height of the discarded material at the upper part does not change, the shear resistance and the resultant shear force of the side interface are $2T_1$ and $2T_2$. According to the Mohr–Coulomb strength criterion:

$$T = 2 \iint\limits_{A} \left(\sigma \tan \varphi_{\mathrm{m}} + c_{\mathrm{m}} \right) \mathrm{d}A$$
(1)

where φ_{m} is the internal friction angle of the coal pillar, c_{m} is the cohesion of the coal pillar, *A* is the area of the coal pillar side interface, and σ is the normal stress acting on the side interface of the coal pillar.

As the height of the supporting coal pillar is fixed in its strike direction, the self-weight stress at the same level of any section (such as sections *GE'*, *PE'*, *QF'*, and *KF'* in Fig. 4) is the same as the Poisson effect (G_1, P_1, Q_1, K_1). Therefore, the shear resistance *T* is only related to the section area. According to the triangular function relationship, the section where the supporting coal pillar is most likely to undergo shear failure is the vertical plane that crosses the end of the supporting coal pillar at its bottom interface. Taking into account the horizontal base and the inclined base, the spatial shape of the supporting coal pillar can be approximated as a quadrangular prism with a quadrilateral cross-section.
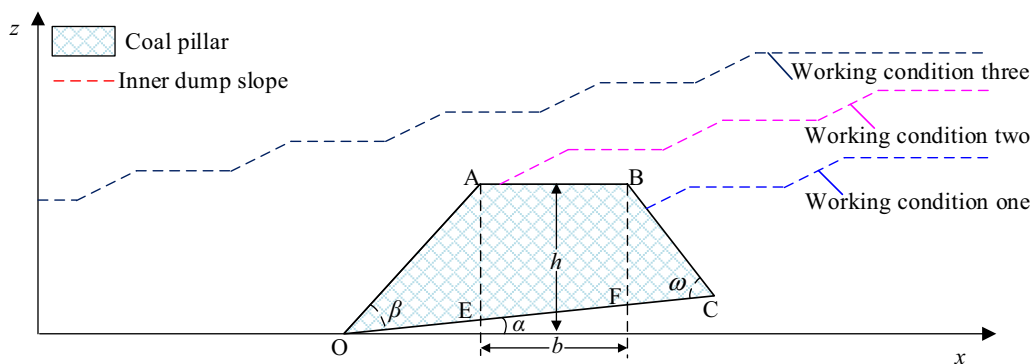

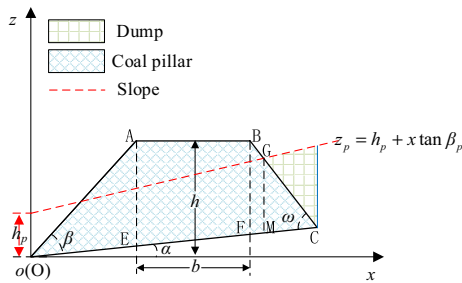**Fig. 5** Section indication under three working conditions

Fig. 6 Development of dumping to coal pillar side

According to the limit equilibrium condition in the x-direction:

$$F = S + T_1 + T_2 \tag{2}$$

Thus, the condition for the coal pillar to remain stable and exert the maximum supporting effect is $F < S + T_1 + T_2$. Therefore, the supporting effect of the coal pillar is three-dimensional, and its magnitude is $S + T_1 + T_2$. As the ratio of the width of the coal pillar to the length of the end slope on both sides is small, additional force is generated by the triangular vertical load (Shao and Wei 1998). This implies that S is determined by the self-weight of the supporting coal

supporting coal pillar, (2) development of the dumping to the top surface of the supporting coal pillar, and (3) development of the entire supporting coal pillar for dumping. The cross-sections of each working condition are shown in Fig. 5. Corner points B and A of the top surface of the supporting coal pillar denote the boundary points of working conditions I and II, and of working conditions II and III, respectively.

According to the coal pillar morphological parameters, coal pillar height equations $H_I(x)$, $H_{II}(x)$, and $H_{III}(x)$ are established as follows for areas AOE, $AEBF$, and BFC, respectively:

$$\begin{cases} H_I(x) = x \tan(\beta + \alpha), x \subseteq \left[0, \dfrac{h}{\tan(\beta+\alpha)}\right] \\ H_{II}(x) = h, x \subseteq \left[\dfrac{h}{\tan(\beta+\alpha)}, b + \dfrac{h}{\tan(\beta+\alpha)}\right] \\ H_{III}(x) = h + \left[b + \dfrac{h}{\tan(\beta+\alpha)} - x\right] \tan(\omega - \alpha) \\ x \subseteq \left\{b + \dfrac{h}{\tan(\beta+\alpha)}, \dfrac{h + \left[\dfrac{h}{\tan(\beta+\alpha)} + b\right] \tan(\omega-\alpha)}{\tan(\omega-\alpha) + \tan\alpha}\right\} \end{cases} \tag{3}$$

The slope equation of the inner dump is z_p, and the base morphological equation of the inner dump is $H_d(x)$:

$$\begin{cases} z_p = h_p + x \tan\beta_p \\ H_d(x) = x \tan\alpha, x \subseteq \left(0, h + \left[\dfrac{h}{\tan(\beta+\alpha)} + b\right] \tan(\omega - \alpha) / [\tan(\omega - \alpha) + \tan\alpha]\right) \end{cases} \tag{4}$$

pillar and the load of the upper waste, the morphological parameters of the bottom interface of the supporting coal pillar, and the lithology of the inner dump base. T is determined by the normal stress of the side interface, the properties of the supporting coal pillar, and the morphological parameters of the site interface.

2.2 Characterization of three-dimensional mechanical effects of supporting coal pillar

The three-dimensional supporting effect of the coal pillar is affected by the load of the upper waste. Thus, it is necessary to characterize the three-dimensional mechanical effect of the coal pillar in the inner dump at different development positions. In this study, three working conditions were considered: (1) development of the dumping to the side of the

2.2.1 Three-dimensional supporting effect under the development of dumping to coal pillar side

Taking the outer corner of the coal pillar bottom interface as the origin of the coordinates, the trapezoidal section is divided into four areas: the triangle AOE, trapezoid AEFB, quadrilateral BFMG, and triangle GMC. The area division is shown in Fig. 6. The shear resistance T of the interface on both sides of the end slope is twice the sum of the side interface shear resistance of the four regions, and the bottom interface shear resistance S is the sum of the bottom interface shear resistance of the four regions.

(1) Shear resistance T of side interface.

The shear resistance of the side interface in AOE is T, that in AEBF is T, that in BFMG is T, and that in GMC is T'. These quantities can be written as follows:

$$
\begin{cases}
T_{\mathrm{I}} = \int_0^{\frac{h}{\tan(\beta+\alpha)}} \int_{x\tan\alpha}^{x\tan(\beta+\alpha)} \left\{ \tan\varphi_{\mathrm{m}} k\gamma_{\mathrm{m}}\left[H_{\mathrm{I}}(x)-z\right]+c_{\mathrm{m}} \right\} \mathrm{d}z\mathrm{d}x \\[2mm]
T_{\mathrm{II}} = \int_{\frac{h}{\tan(\beta+\alpha)}}^{\frac{h}{\tan(\beta+\alpha)}+b} \int_{x\tan\alpha}^{h} \left\{ \tan\varphi_{\mathrm{m}} k\gamma_{\mathrm{m}}\left[H_{\mathrm{II}}(x)-z\right]+c_{\mathrm{m}} \right\} \mathrm{d}z\mathrm{d}x \\[2mm]
T_{\mathrm{III}} = \int_{\frac{h}{\tan(\beta+\alpha)}+b}^{\frac{h+\left[\frac{h}{\tan(\beta+\alpha)}+b\right]\tan(\omega-\alpha)-h_{\mathrm{p}}}{\tan\beta_{\mathrm{p}}+\tan(\omega-\alpha)}} \int_{x\tan\alpha}^{h+\left[b+\frac{h}{\tan(\beta+\alpha)}-x\right]\tan(\omega-\alpha)} \left\{ k\tan\varphi_{\mathrm{m}}\gamma_{\mathrm{m}}\left[H_{\mathrm{III}}(x)-z\right]+c_{\mathrm{m}} \right\} \mathrm{d}z\mathrm{d}x \\[2mm]
T'_{\mathrm{III}} = \int_{\frac{h+\left[\frac{h}{\tan(\beta+\alpha)}+b\right]\tan(\omega-\alpha)-h_{\mathrm{p}}}{\tan\beta_{\mathrm{p}}+\tan(\omega-\alpha)}}^{\frac{h+\left[\frac{h}{\tan(\beta+\alpha)}+b\right]\tan(\omega-\alpha)}{\tan(\omega-\alpha)+\tan\alpha}} \int_{x\tan\alpha}^{h+\left[b+\frac{h}{\tan(\beta+\alpha)}-x\right]\tan(\omega-\alpha)} \left\{ \tan\varphi_m k\left\{ \begin{array}{l} \gamma_{\mathrm{m}}\left[H_{\mathrm{III}}(x)-z\right] \\ +\gamma_{\mathrm{p}}\left[z_{\mathrm{p}}-H_{\mathrm{III}}(x)\right] \end{array} \right\}+c_{\mathrm{m}} \right\} \mathrm{d}z\mathrm{d}x
\end{cases}
\tag{5}
$$

(2) Shear resistance S of the bottom interface.

The shear resistance of the bottom interface in AOE is S_{I}, that in AEBF is S_{II}, that in BFMG is S_{III}, and that in GMC is S'_{III}. These quantities can be written as follows:

Based on Eqs. (5) and (6), the three-dimensional supporting effect under the development of dumping to the coal pillar side is given by:

$$
\begin{cases}
S_{\mathrm{I}} = \int_0^d \int_0^{\frac{h}{\tan(\beta+\alpha)}} \tan\varphi_j\gamma_{\mathrm{m}}[x\tan(\beta+\alpha)-x\tan\alpha]\mathrm{d}x\mathrm{d}y + \int_0^d \int_0^{\frac{h}{\cos\alpha\tan(\beta+\alpha)}} c_j\mathrm{d}x\mathrm{d}y \\[2mm]
S_{\mathrm{II}} = \int_0^d \int_{\frac{h}{\tan(\beta+\alpha)}}^{\frac{h}{\tan(\beta+\alpha)}+b} \tan\varphi_j\gamma_{\mathrm{m}}(h-x\tan\alpha)\mathrm{d}x\mathrm{d}y + \int_0^d \int_{\frac{h}{\cos\alpha\tan(\beta+\alpha)}}^{\frac{h}{\cos\alpha\tan(\beta+\alpha)}+\frac{b}{\cos\alpha}} c_j\mathrm{d}x\mathrm{d}y \\[2mm]
S_{\mathrm{III}} = \int_0^d \int_{A_7}^{A_{10}} \tan\varphi_j\gamma_{\mathrm{m}}\left\{ h+\left[A_7-x\right]\tan(\omega-\alpha)-x\tan\alpha \right\}\mathrm{d}x\mathrm{d}y + \int_0^d \int_{\frac{A_7}{\cos\alpha}}^{\frac{A_{10}}{\cos\alpha}} c_j\mathrm{d}x\mathrm{d}y \\[2mm]
S'_{\mathrm{III}} = \int_0^d \int_{A_{10}}^{A_8} \tan\varphi_{\mathrm{m}}\left\{ \gamma_{\mathrm{m}}\left[A_6-A_5x-A_3x\right]+\gamma_{\mathrm{p}}\left[h_{\mathrm{p}}+xA_4+xA_5-A_6\right] \right\}\mathrm{d}x\mathrm{d}y + \frac{dc_j}{\cos\alpha}(A_8-A_{10})
\end{cases}
\tag{6}
$$

where

$$
S+T = 2\left(T_{\mathrm{I}}+T_{\mathrm{II}}+T_{\mathrm{III}}+T'_{\mathrm{III}}\right)+\left(S_{\mathrm{I}}+S_{\mathrm{II}}+S_{\mathrm{III}}+S'_{\mathrm{III}}\right)
\tag{7}
$$

$$
\begin{cases}
A_3 = \tan\alpha \\
A_4 = \tan\beta_{\mathrm{p}} \\
A_5 = \tan(\omega-\alpha) \\
A_6 = h+\tan(\omega-\alpha)\left[h/\tan(\beta+\alpha)+b\right] \\
A_7 = h/\tan(\beta+\alpha)+b \\
A_8 = \left\{ h+\tan(\omega-\alpha)\left[h/\tan(\beta+\alpha)+b\right] \right\}/\left[\tan\alpha+\tan(\omega-\alpha)\right] \\
A_{10} = \left\{ h+\tan(\omega-\alpha)\left[h/\tan(\beta+\alpha)+b\right]-h_{\mathrm{p}} \right\}/\left[\tan\beta_{\mathrm{p}}+\tan(\omega-\alpha)\right]
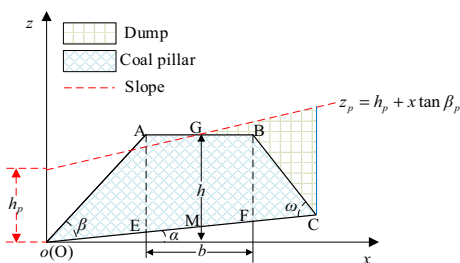\end{cases}
$$

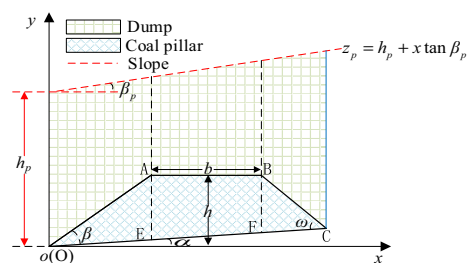**Fig. 7** Development of dumping to coal pillar top

Fig. 8 Development of dumping to entire coal pillar

2.2.2 Three-dimensional supporting effect under the development of dumping to coal pillar top

Because the side interface shear force and bottom interface shear force of the triangular AOE area are the same for the development of dumping to the coal pillar side and to the coal pillar top, we need only consider the other regions here. The regional division is shown in Fig. 7.

(1) Shear resistance T of side interface.

The shear resistance of the side interface in AEMG is $T_{2\mathrm{II}}$, that in GMFB is $T'_{2\mathrm{II}}$, and that in BFC is $T_{2\mathrm{III}}$. These quantities can be written as follows:

$$
\begin{cases}
T_{2\mathrm{II}} = \int_{\frac{h}{\tan(\beta+\alpha)}}^{\frac{h-h_\mathrm{p}}{\tan\beta_\mathrm{p}}} \int_{x\tan\alpha}^{h} \left[\tan\varphi_\mathrm{m} k\gamma_\mathrm{m}(h-z) + c_\mathrm{m}\right] \mathrm{d}z\mathrm{d}x \\
T'_{2\mathrm{II}} = \int_{\frac{h-h_\mathrm{p}}{\tan\beta_\mathrm{p}}}^{\frac{h}{\tan(\beta+\alpha)}+b} \int_{x\tan\alpha}^{h} \left\{\tan\varphi_\mathrm{m} k\left[\gamma_\mathrm{m}(h-z) + \gamma_\mathrm{p}\left(h_\mathrm{p} + x\tan\beta_\mathrm{p} - h\right)\right] + c_\mathrm{m}\right\} \mathrm{d}z\mathrm{d}x \\
T_{2\mathrm{III}} = \int_{A_7}^{A_8} \int_{x\tan\alpha}^{h+\left[b+\frac{h}{\tan(\beta+\alpha)}-x\right]\tan(\omega-\alpha)} \left\{k\tan\varphi_\mathrm{m} \begin{bmatrix} \gamma_\mathrm{m}\left(A_6 - A_5 x - z\right) \\ +\gamma_\mathrm{p}\left(h_\mathrm{p} + A_4 x + A_5 x - A_6\right) \end{bmatrix} + c_\mathrm{m}\right\} \mathrm{d}z\mathrm{d}x
\end{cases}
\tag{8}
$$

(2) Shear resistance S of the bottom interface.

The shear resistance of the bottom interface in AEMG is $S_{2\mathrm{II}}$, that in GMFB is $S'_{2\mathrm{II}}$, and that in BFC is $S_{2\mathrm{III}}$. These quantities can be written as follows:

$$
\begin{cases}
S_{2\mathrm{II}} = \int_0^d \int_{\frac{h}{\tan(\beta+\alpha)}}^{\frac{h-h_\mathrm{p}}{\tan\beta_\mathrm{p}}} \tan\varphi_j \gamma_\mathrm{m}(h - x\tan\alpha)\mathrm{d}x\mathrm{d}y + \int_0^d \int_{\frac{A_1}{\cos\alpha}}^{\frac{A_9}{\cos\alpha}} c_j \mathrm{d}x\mathrm{d}y \\
S'_{2\mathrm{II}} = \int_0^d \int_{\frac{h-h_\mathrm{p}}{\tan\beta_\mathrm{p}}}^{\frac{h}{\tan(\beta+\alpha)}+b} \tan\varphi_j \left[\gamma_\mathrm{m}(h - x\tan\alpha) + \gamma_\mathrm{p}\left(h_\mathrm{p} + x\tan\beta_\mathrm{p} - h\right)\right] \mathrm{d}x\mathrm{d}y \\
S_{2\mathrm{III}} = \int_0^d \int_{A_7}^{A_8} \tan\varphi_j \begin{bmatrix} \gamma_\mathrm{m}\left(A_6 - A_5 x - A_3 x\right) \\ +\gamma_\mathrm{p}\left(h_\mathrm{p} + A_4 x + A_5 x - A_6\right) \end{bmatrix} \mathrm{d}x\mathrm{d}y + \int_0^d \int_{\frac{A_7}{\cos\alpha}}^{\frac{A_8}{\cos\alpha}} c_j \mathrm{d}x\mathrm{d}y
\end{cases}
\tag{9}
$$

where $A_9 = \left(h - h_\mathrm{p}\right)/\tan\beta_\mathrm{p}$.

Based on Eqs. (8) and (9), the three-dimensional supporting effect under the development of dumping to the coal pillar top is given by:

$$
S + T = 2\left(T_\mathrm{I} + T_{2\mathrm{II}} + T'_{2\mathrm{II}} + T_{2\mathrm{III}}\right) + \left(S_\mathrm{I} + S_{2\mathrm{II}} + S'_{2\mathrm{II}} + S_{2\mathrm{III}}\right)
\tag{10}
$$

2.2.3 Three-dimensional supporting effect under the development of dumping to entire coal pillar

The mechanical boundary of the side interface and the bottom interface of the triangular BFC area under the development of dumping to the coal pillar top is different from that in the case of development of dumping to the entire coal pillar. In particular, the shear resistance can be expressed Eqs. (8) and (9). We now derive expressions for the other areas. The regional division is shown in Fig. 8.

(1) Shear resistance T of side interface.

The shear resistance of the side interface in AOE is $T_{3\mathrm{I}}$ and that in AEFB is $T_{3\mathrm{II}}$. These quantities can be written as follows:

$$
\begin{cases}
T_{3\mathrm{I}} = \int_0^{\frac{h}{\tan(\beta+\alpha)}} \int_{x\tan\alpha}^{x\tan(\beta+\alpha)} \tan\varphi_\mathrm{m} k \left\{ \begin{array}{l} \gamma_\mathrm{m}[x\tan(\beta+\alpha) - z] \\ +\gamma_\mathrm{p}\left[z_\mathrm{p} - x\tan(\beta+\alpha)\right] + c_\mathrm{m} \end{array} \right\} \mathrm{d}z\mathrm{d}x \\
T_{3\mathrm{II}} = \int_{\frac{h}{\tan(\beta+\alpha)}}^{\frac{h}{\tan(\beta+\alpha)}+b} \int_{x\tan\alpha}^{h} \left\{\tan\varphi_\mathrm{m} k\left[\gamma_\mathrm{m}(h-z) + \gamma_\mathrm{p}(z_\mathrm{p} - h)\right] + c_\mathrm{m}\right\} \mathrm{d}z\mathrm{d}x
\end{cases}
\tag{11}
$$

where $A_2 = \tan(\beta + \alpha)$.

(2) Shear resistance S of bottom interface.

The shear resistance of the bottom interface in AOE is $S_{3\mathrm{I}}$ and that in AEFB is $S_{3\mathrm{II}}$. These quantities can be written as follows:

$$\left\{ \begin{array}{l} S_{3\mathrm{I}} = \int_0^d \int_0^{\frac{h}{\tan(\beta+\alpha)}} \tan\varphi_j \left\{ \begin{array}{l} \gamma_{\mathrm{m}}[x\tan(\beta+\alpha) - x\tan\alpha] \\ +\gamma_{\mathrm{p}}[h_{\mathrm{p}} + x\tan\beta_{\mathrm{p}} - x\tan(\beta+\alpha)] \end{array} \right\} \mathrm{d}x\mathrm{d}y + \int_0^d \int_0^{\frac{h}{\cos\alpha\tan(\beta+\alpha)}} c_j\mathrm{d}x\mathrm{d}y \\ S_{3\mathrm{II}} = \int_0^d \int_{\frac{h}{\tan(\beta+\alpha)}}^{\frac{h}{\tan(\beta+\alpha)}+b} \tan\varphi_j \left[\begin{array}{l} \gamma_{\mathrm{m}}(h - x\tan\alpha) \\ +\gamma_{\mathrm{p}}(h_{\mathrm{p}} + x\tan\beta_{\mathrm{p}} - h) \end{array} \right] \mathrm{d}x\mathrm{d}y + \int_0^d \int_{\frac{h}{\cos\alpha\tan(\beta+\alpha)}}^{\frac{h}{\cos\alpha\tan(\beta+\alpha)}+\frac{b}{\cos\alpha}} c_j\mathrm{d}x\mathrm{d}y \end{array} \right. \tag{12}$$

Based on Eqs. (11) and (12), the three-dimensional supporting effect under the development of dumping to the entire coal pillar is given by:

$$S + T = 2(T_{2\mathrm{III}} + T_{3\mathrm{I}} + T_{3\mathrm{II}}) + (S_{2\mathrm{III}} + S_{3\mathrm{I}} + S_{3\mathrm{II}}) \tag{13}$$

We have established mathematical expressions for the three-dimensional supporting effect of the coal pillar when the inner dump is developed in different engineering positions. As a result, a quantitative characterization of the three-dimensional mechanical effect of the supporting coal pillar of the inner dump has been realized.

In engineering applications, it is first necessary to select a reasonable calculation method according to the location of the project development. Using the design parameters of the open-pit coal mine and the physical and mechanical parameters of the rock and soil, the mechanical effects of the supporting coal pillar can be analyzed.

3 Two-dimensional equivalent method for determining the supporting effect of the coal pillar

The inner dump slope is homogeneous and loose. There is little evidence of force from the end slope on both sides, and so this can be neglected as a first approximation. The resulting formulation can be regarded as a plane strain problem. Therefore, the two-dimensional rigid body limit equilibrium method can be used for analysis. To apply this approach to engineering, we need to transform the three-dimensional supporting effect into a two-dimensional effect. Obviously, the three-dimensional supporting effect of the coal pillar is the combined shear force of the side interface and the bottom interface. When the two-dimensional rigid body limit equilibrium method is used, the supporting effect of the coal pillar is only reflected in the shearing force of the bottom interface. Finding a suitable method for equating the shear force on the side interface to the bottom interface will result

in the two-dimensional equivalent of the three-dimensional supporting effect.

Based on Eqs. (5)–(12), the three-dimensional supporting effect of the coal pillar is essentially the resultant force of the cohesion and internal frictional resistance between the side interface and the bottom interface. These components are provided by the cohesion and the internal friction angle of the shear strength parameters. The former is only related to the morphological parameters of the coal pillar, and the latter is affected by the vertical external load above the coal pillar due to the development of the dumping project. This is influenced by the composition type of the shear reaction force at the bottom interface of the block in the two-dimensional rigid body limit equilibrium method, which is consistent with the influencing factors. Therefore, the equivalent cohesion of the bottom interface and the equivalent internal friction angle (or the equivalent internal friction angle coefficient) can be solved by combining similar terms to achieve the two-dimensional equivalent of the pillar supporting effect.

(1) Equivalent cohesion c_d.

The shear reaction force provided by the cohesive force is independent of the load of the dump material. Thus, this force is only related to the cohesive force of the supporting coal pillar and its morphological parameters, and the cohesive force of the base rock of the inner dump. The equivalent cohesion c_d under the three working conditions can be written as follows:

$$c_{d1} = \frac{c_{\mathrm{m}}\cos\alpha \left\{ \begin{array}{l} A_1^2(A_2 - A_3) + b(2h - 2A_1A_3 - bA_3) \\ +(A_7 - A_8)[(A_5 + A_3)(A_7 + A_8) - 2A_6] \end{array} \right\}}{d\left[A_1 + b + \left(\frac{h + A_5A_7}{A_3 + A_5} - A_7\right)\right]} + c_j \tag{14}$$

where $A_1 = h/\tan(\beta+\alpha)$.

(2) Equivalent internal friction coefficient $\tan\varphi_d$.

The equivalent internal friction coefficient $\tan\varphi_{d_{11}}$ under the development of dumping to the coal pillar side can be written as follows:

$$\tan \varphi_{d11} = \frac{k \tan \varphi_{\mathrm{m}}}{3d} \frac{\left\{ \begin{array}{c} \dfrac{h^3[\tan(\beta+\alpha)-\tan\alpha]^2}{\tan^3(\beta+\alpha)} \\ +[A_1^3(-A_3^2)+3A_1^2A_3h-3A_1h^2+A_7(A_3^2A_7^2-3A_3A_7h+3h^2)] \\ +(A_3+A_5)^2(A_8^3-A_7^3)+3A_6(A_3+A_5)(A_7^2-A_8^2)+3A_6^2(A_8-A_7)] \\ +\dfrac{\gamma_{\mathrm{p}}}{\gamma_{\mathrm{m}}}(A_{10}-A_8)\left\{ \begin{array}{c} (A_3+A_5)[2(A_5+A_4)(A_{10}^2+A_{10}A_8+A_8^2)+3h_{\mathrm{p}}(A_{10}+A_8)] \\ +3A_6(A_8-A_{10})(A_3+2A_5+A_4)-6A_6h_{\mathrm{p}}+6A_6^2 \end{array} \right\} \end{array} \right\}}{\left\{ \begin{array}{c} \dfrac{h^2[\tan(\beta+\alpha)-\tan\alpha]}{\tan^2(\beta+\alpha)}+b\left\{\left[\dfrac{2h}{\tan(\beta+\alpha)}+b\right]\tan\alpha-2h\right\} \\ +2\left[(A_3+A_5)(\dfrac{A_7^2}{2}-\dfrac{A_8^2}{2})+A_6(A_8-A_7)\right] \\ +\dfrac{\gamma_{\mathrm{p}}}{\gamma_{\mathrm{m}}}(A_8-A_{10})[A_4(A_{10}+A_8)+A_5A_{10}+A_5A_8+2h_{\mathrm{p}}-2A_6] \end{array} \right\}} + \tan\varphi_j \quad (15)$$

The equivalent internal friction coefficient $\tan \varphi_{d_{21}}$ under the development of dumping to the coal pillar top can be written as follows:

$$\tan \varphi_{d21} = \frac{\tan \varphi_{\mathrm{m}} k}{3d} \frac{\left\{ \begin{array}{c} [-A_1^3A_3^2+3A_1^2A_3h-3A_1h^2+A_9(A_3^2A_9^2-3A_3A_9h+3h^2)] \\ +A_1^3(A_2-A_3)^2 \\ +[A_9^3(-A_3^2)+3A_9^2A_3h-3A_9h^2+A_7(A_3^2A_7^2-3A_3A_7h+3h^2)] \\ +\dfrac{\gamma_{\mathrm{p}}}{\gamma_{\mathrm{m}}}(A_9-A_7)\left\{ \begin{array}{c} A_3[2A_4(A_7^2+A_7A_9+A_9^2)-3(A_9+A_7)(h-h_{\mathrm{p}})] \\ -3h[A_4(A_9+A_7)-2h+2h_p] \end{array} \right\} \\ +\{(A_3+A_5)^2(A_8^3-A_7^3)+3A_6(A_3+A_5)(A_7^2-A_8^2)+3A_6^2(A_8-A_7)\} \\ +\dfrac{\gamma_p(A_7+A_8)}{\gamma_m}\left\{ \begin{array}{c} (A_3+A_5)[2(A_5+A_4)(A_7^2+A_7A_8+A_8^2)+3h_{\mathrm{p}}(A_7+A_8)] \\ -3A_6(A_7-A_8)(A_3+2A_5+A_4)-6A_6h_{\mathrm{p}}+6A_6^2 \end{array} \right\} \end{array} \right\}}{\left\{ \begin{array}{c} A_1^2(A_2-A_3)+(A_1-A_9)(A_1A_3+A_9A_3-2h) \\ +(A_9-A_7)(A_9A_3+A_7A_3-2h) \\ +\dfrac{\gamma_{\mathrm{p}}}{\gamma_{\mathrm{m}}}(A_7-A_9)(A_7A_4+A_9A_4-2h+2h_{\mathrm{p}}) \\ +2\left[-(A_5+A_3)(\dfrac{A_8^2}{2}-\dfrac{A_7^2}{2})+A_6(A_8-A_7)\right] \\ -\dfrac{\gamma_{\mathrm{p}}}{\gamma_{\mathrm{m}}}(A_7-A_8)(A_4(A_7+A_8)+A_5A_7+A_5A_8+2h_{\mathrm{p}}-2A_6) \end{array} \right\}} + \tan\varphi_j \quad (16)$$

The equivalent internal friction coefficient $\tan \varphi_{d_{31}}$ under the development of dumping to the entire coal pillar can be written as follows:

$$\tan \varphi_{d31} = \frac{\tan \varphi_{\mathrm{m}} k}{3d} \frac{\left\{ \begin{array}{l} A_1^3(A_2 - A_3)^2 - \dfrac{\gamma_{\mathrm{p}}}{\gamma_{\mathrm{m}}} A_1^2(A_2 - A_3)\left[2A_1(A_2 - A_4) - 3h_{\mathrm{p}}\right] \\[6pt] b\left[3A_1^2 A_3^2 + 3A_1 A_3(bA_3 - 2h) + b^2 A_3^2 - 3bA_3 h + 3h^2\right] \\[6pt] + \dfrac{\gamma_{\mathrm{p}}}{\gamma_{\mathrm{m}}} b \left\{ \begin{array}{l} -6A_1^2 A_3 A_4 + 6A_1\left[A_3(-bA_4 + h - h_{\mathrm{p}}) + hA_4\right] \\ -2b^2 A_3 A_4 + 3b(A_3 h - A_3 h_{\mathrm{p}} + hA_4) + 6h(h_{\mathrm{p}} - h) \end{array} \right\} \\[12pt] + \left[(A_3 + A_5)^2(A_8^3 - A_7^3) + 3A_6(A_3 + A_5)(A_7^2 - A_8^2) + 3A_6^2(A_8 - A_7)\right] \\[6pt] + \dfrac{\gamma_{\mathrm{p}}}{\gamma_{\mathrm{m}}}(A_7 - A_8) \left\{ \begin{array}{l} (A_3 + A_5)\left[2(A_5 + A_4)(A_7^2 + A_7 A_8 + A_8^2) + 3h_{\mathrm{p}}(A_7 + A_8)\right] \\ -3A_6(A_7 - A_8)(A_3 + 2A_5 + A_4) - 6A_6 h_{\mathrm{p}} + 6A_6^2 \end{array} \right\} \end{array} \right\}}{\left\{ \begin{array}{l} A_1^2(A_2 - A_3) + \dfrac{\gamma_{\mathrm{p}}}{\gamma_{\mathrm{m}}} A_1\left[A_1(A_4 - A_2) + 2h_{\mathrm{p}}\right] \\[6pt] + b(A_1 A_3 + A_7 A_3 - 2h) + \dfrac{\gamma_{\mathrm{p}}}{\gamma_{\mathrm{m}}} b(A_1 A_4 + A_7 A_4 - 2h + 2h_{\mathrm{p}}) \\[6pt] + 2\left[(-A_3 - A_5)(\dfrac{A_8^2}{2} - \dfrac{A_7^2}{2}) + A_6(A_8 - A_7)\right] \\[6pt] - \dfrac{\gamma_{\mathrm{p}}}{\gamma_{\mathrm{m}}}(A_7 - A_8)\left[A_4(A_7 + A_8) + A_5 A_7 + A_5 A_8 + 2h_{\mathrm{p}} - 2A_6\right] \end{array} \right\}} + \tan \varphi_j \tag{17}$$

4 Calculation method of slope stability of inner dump under coal pillar support

Slope stability analysis is commonly performed using the residual thrust method (Feng et al. 2014; Zhou et al. 2019; Ram et al. 2019). Also called the transfer coefficient method or the unbalanced force method, this is suitable for determining the stability coefficient of any slip surface. Here, the two-dimensional equivalent shear strength parameters are introduced into the residual thrust method, and a method for calculating the slope stability of the inner dump slope under the effect of coal pillar support and taking into account the development position of dumping is established.

The shapes of the slope and the supporting coal pillar are shown in Fig. 9. The landslide model is a circular arc–base combined sliding formulation in which the sliding mass is divided into several vertical blocks. To ensure the accuracy of the calculations, the blocks near the supporting coal pillar need to be encrypted, and the inflection point of the slope step, intersection point of the sliding surfaces, and the rock layer need to be divided into separate blocks.

Under arc–base combined sliding, the bottom surface of the upper blocks on the circular sliding surface is different from that of the upper blocks on the base sliding surface. Therefore, the circular sliding surface mass is divided into a total of n blocks. The upper sliding mass is divided into k blocks and the upper base sliding mass is divided into nk blocks; there are u blocks containing coal pillars, n-k-u blocks without coal pillars, and q blocks from the inner corner of the coal pillar to the intersection of the circular arc sliding surface and the base sliding surface.

(1) Residual thrust of the upper blocks on the arc sliding surface.

Let us consider block i on the upper part of the arc sliding surface, $i = 0, 1, \ldots, k$. The bottom inclination of block i is δ_i, the bottom inclination of block i-1 is $\delta_{i_{-1}}$, the residual thrust of block i is D_i, and the residual thrust of block i-1 is D_{i-1}.

Then, the equilibrium equation for the direction parallel to the bottom of block i can be established as:

$$D_i = W_i \sin \delta_i + D_{i-1} \cos(\delta_{i-1} - \delta_i) - S_i \tag{18}$$

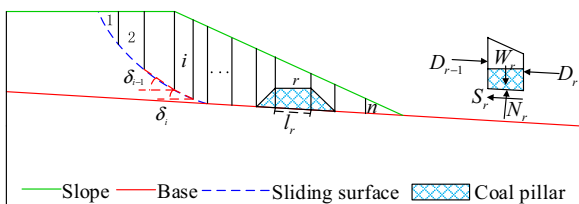where W_i is the weight of block i and S_i is the tangential force at the bottom of block i.

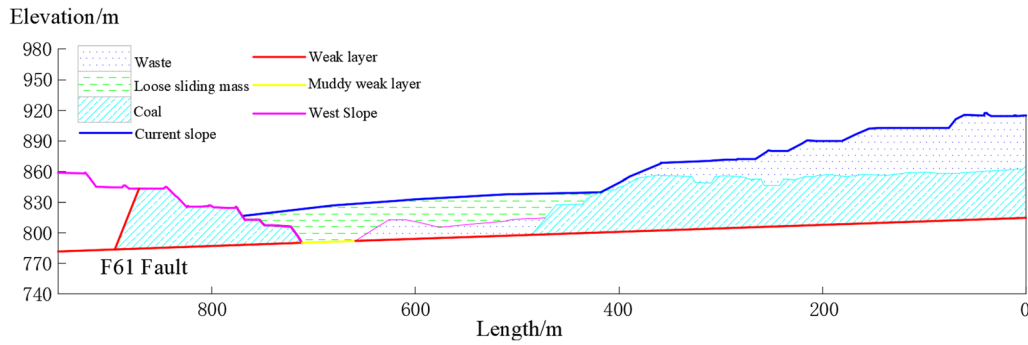**Fig. 9** Slope and supporting coal pillar shapes

Fig. 10 Typical engineering geology of inner dump

The equilibrium equation for the direction perpendicular to the bottom of block i is:

$$N_i = W_i \cos \delta_i + D_{i-1} \sin(\delta_{i-1} - \delta_i) \tag{19}$$

where N_i is the normal force at the bottom of block i.

According to the Moore–Coulomb strength criterion (Cai et al. 2013; Yuan et al. 2019; Naeini et al. 2012):

$$S_i = \frac{c_i l_i + N_i \tan \varphi_i}{K} \tag{20}$$

where l_i is the length of the bottom of block i, c_i is the cohesion of the bottom of block i, φ_i is the internal friction angle of the bottom of block i, and K is the reduction coefficient.

Based on Eqs. (18)–(20), the residual thrust of block i is given by:

$$D_i = W_i \sin \delta_i + D_{i-1} \cos(\delta_{i-1} - \delta_i) - \frac{c_i l_i + \left[W_i \cos \delta_i + D_{i-1} \sin(\delta_{i-1} - \delta_i) \right] \tan \varphi_i}{K} \tag{21}$$

The residual thrust D_k of the upper sliding mass on the arc sliding surface can then be written as follows:

$$\begin{cases} D_2 = W_2 \sin \delta_2 + D_1 \cos(\delta_1 - \delta_2) - \frac{c_2 l_2 + \left[W_2 \cos \delta_2 + D_1 \sin(\delta_1 - \delta_2) \right] \tan \varphi_2}{K} \\ D_3 = W_3 \sin \delta_3 + D_2 \cos(\delta_2 - \delta_3) - \frac{c_3 l_3 + \left[W_3 \cos \delta_3 + D_2 \sin(\delta_2 - \delta_3) \right] \tan \varphi_3}{K} \\ \qquad\qquad \cdots\cdots \\ D_k = W_k \sin \delta_k + D_{k-1} \cos(\delta_{k-1} - \delta_k) - \frac{c_k l_k + \left[W_k \cos \delta_k + D_{k-1} \sin(\delta_{k-1} - \delta_k) \right] \tan \varphi_k}{K} \end{cases} \tag{22}$$

(2) Residual thrust of the upper blocks with coal pillars on the base sliding surface.

Let us consider block r with a coal pillar on the base sliding surface, $r = 0, 1, \ldots, u$. We assume that the base inclination angle of the inner dump is α:

$$\delta_1 = \delta_2 \ldots = \delta_u = \alpha \tag{23}$$

Table 1 Geotechnical physical mechanics indices

Strata	c (kPa)	φ (°)	γ (kN/m³)
Coal	70	24	13.1
Loose sliding mass	0	14	19.0
Muddy weak layer	0	6.8	17.0
Weak layer	10	10	17.0
Waste	15.13	14	19.0

The equilibrium equation for the direction parallel to the bottom of block r can be written as:

$$D_r = W_r \sin \alpha + D_{r-1} - S_r \tag{24}$$

where W_r is the weight of block r, given by:

$$W_r = A_{rm} \gamma_m + (A_r - A_{rm}) \gamma_p \tag{25}$$

The equilibrium equation for the direction perpendicular to the bottom of block r is given by:

$$N_r = W_r \cos \alpha \tag{26}$$

According to the Moore–Coulomb strength criterion:

$$S_r = \frac{c_d l_r + N_r \tan \varphi_d}{K} \tag{27}$$

Table 2 Orthogonal test calculation results of inner dump stability

Test number	h (m)	b (m)	d (m)	β (°)	ω (°)	α (°)	h_p (m)	β_p (°)	F_s
1	10	0	100	23	22	0	40	12	1.26
2	10	10	300	27	26	2	45	14	1.06
3	10	20	500	31	30	4	50	16	0.91
4	10	30	700	35	34	6	55	18	0.80
5	20	0	100	27	26	4	50	18	0.86
6	20	10	300	23	22	6	55	16	0.90
7	20	20	500	35	34	0	40	14	1.10
8	20	30	700	31	30	2	45	12	1.23
9	30	0	300	31	34	0	45	16	0.99
10	30	10	100	35	30	2	40	18	0.92
11	30	20	700	23	26	4	55	12	1.19
12	30	30	500	27	22	6	50	14	1.01
13	40	0	300	35	30	4	55	14	1.06
14	40	10	100	31	34	6	50	12	1.28
15	40	20	700	27	22	0	45	18	0.90
16	40	30	500	23	26	2	40	16	0.97
17	10	0	700	23	34	2	50	14	1.06
18	10	10	500	27	30	0	55	12	1.27
19	10	20	300	31	26	6	40	18	0.80
20	10	30	100	35	22	4	45	16	0.93
21	20	0	700	27	30	6	40	16	0.88
22	20	10	500	23	34	4	45	18	0.83
23	20	20	300	35	22	2	50	12	1.24
24	20	30	100	31	26	0	55	14	1.18
25	30	0	500	31	22	2	55	18	0.86
26	30	10	700	35	26	0	50	16	0.97
27	30	20	100	23	30	6	45	14	1.10
28	30	30	300	27	34	4	40	12	1.20
29	40	0	500	35	26	6	45	12	1.14
30	40	10	700	31	22	4	40	14	1.03
31	40	20	100	27	34	2	55	16	1.15
32	40	30	300	23	30	0	50	18	0.98

Table 3 Range analysis of orthogonal tests of inner dump stability

Level	h (m)	b (m)	d (m)	β (°)	ω (°)	α (°)	h_p (m)	β_p (°)
1	1.0113	1.0138	1.0850	1.0362	1.0163	1.0812	1.0200	1.2263
2	1.0275	1.0325	1.0287	1.0412	1.0213	1.0612	1.0225	1.0750
3	1.0300	1.0487	1.0113	1.0350	1.0438	1.0012	1.0387	0.9625
4	1.0638	1.0375	1.0075	1.0200	1.0512	0.9887	1.0512	0.8688
Range	0.0525	0.0350	0.0775	0.0213	0.0350	0.0925	0.0312	0.3575

Thus, the residual thrust of block r is given by:

$$D_r = D_{r-1} + \left[A_{rm}\gamma_m + (A_r - A_{rm})\gamma_p\right]\left(\sin\alpha - \frac{\cos\alpha\tan\varphi_d}{K}\right)$$
$$- \frac{c_d l_r}{K}$$

(3) Residual thrust of the upper blocks without coal pillars on the base sliding surface.

The residual thrust of the upper blocks with and without coal pillars satisfies an equilibrium condition in the parallel and perpendicular directions. The essential difference lies in the tangential force on the bottom surface. Take upper block p without a coal pillar as an example, $p = 1, 2, \ldots, n$-k-u. According to the Moore–Coulomb strength criterion:

🖄 Springer

(28)

Fig. 11 Inner dump stability with respect to various factors (longitudinal intercept of the slope line of the inner dump is determined by the slope angle, the distance from the coal pillar to the slope toe, and the height of the inner dump)
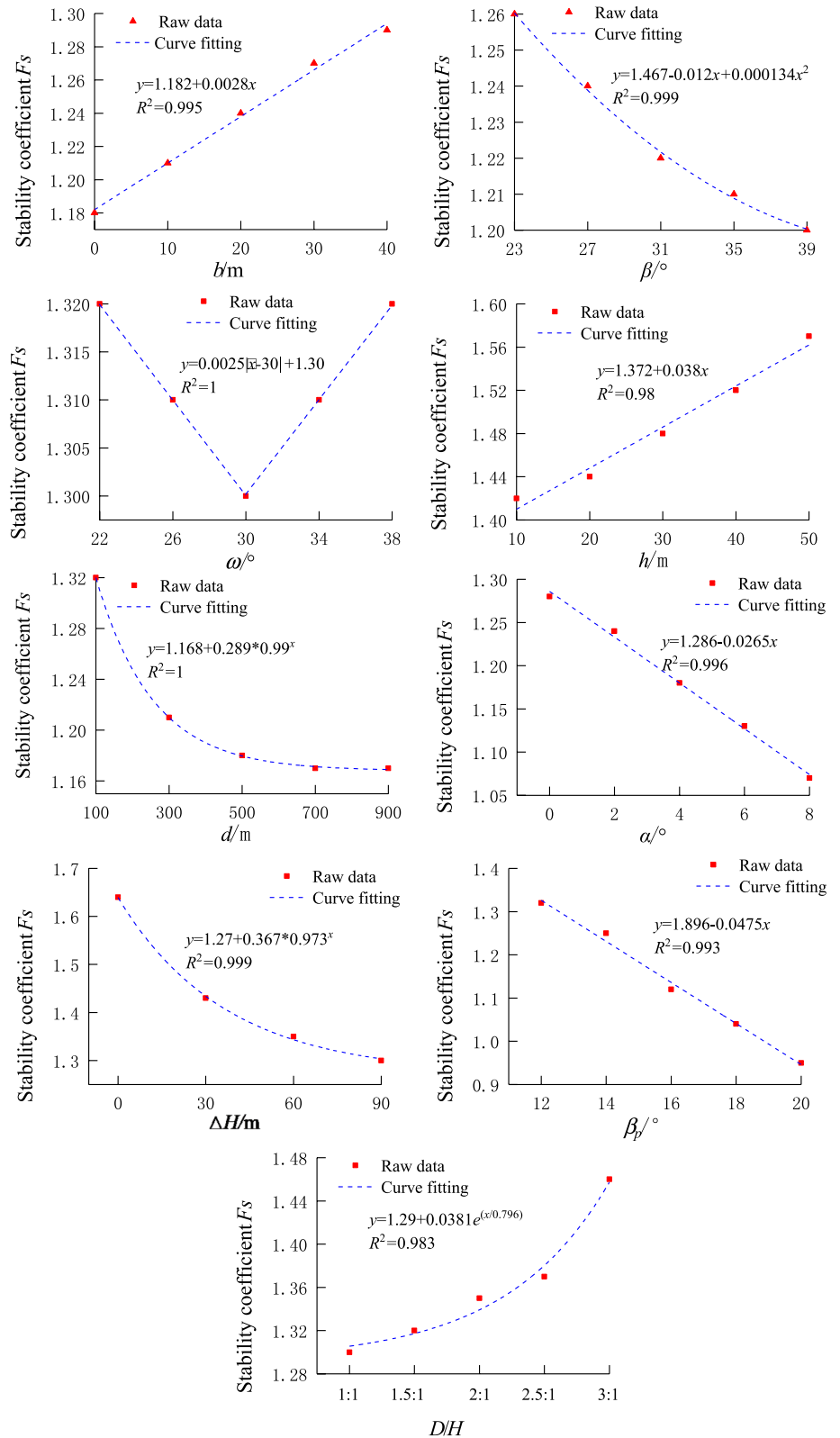
Table 4 Calculation parameters and results under various working conditions

Working condition	β (°)	ω (°)	b (m)	h (m)	h_p (m)	c_d (kPa)	φ (°)	F_s
Condition 1 (Top width set at +816 level)	30	25	0	27.79	17.82	27.00	13.68	1.148
			10	28.15	15.97	28.62	13.86	1.160
			20	28.79	14.12	30.17	14.06	1.178
			30	29.15	12.27	31.37	14.20	1.198
			40	29.79	10.42	32.61	14.36	1.208
Condition 2 (Top width set at +818 level)	31	26	0	29.88	19.74	28.31	13.97	1.155
			10	30.24	17.91	30.01	14.16	1.169
			20	30.60	16.08	31.45	14.33	1.185
			30	30.96	14.25	32.70	14.47	1.205
			40	31.32	12.42	33.81	14.60	1.215
Condition 3 (Top width set at +820 level)	32	27	0	31.97	21.65	29.64	14.26	1.162
			10	32.33	19.84	31.40	14.46	1.176
			20	32.69	18.03	32.91	14.63	1.192
			30	33.05	16.22	34.23	14.78	1.212
			40	33.41	14.41	35.39	14.92	1.222
Condition 4 (Top width set at +822 level)	33	28	0	34.07	23.6	30.97	14.55	1.169
			10	34.43	21.81	32.81	14.75	1.186
			20	34.79	20.02	34.38	14.94	1.199
			30	35.15	18.23	35.76	15.10	1.219
			40	35.50	16.44	36.97	15.24	1.229
Condition 5 (Top width set at +824 level)	34	29	0	36.16	25.54	32.11	14.83	1.176
			10	36.52	23.76	34.21	15.05	1.194
			20	36.88	21.98	35.87	15.24	1.209
			30	37.24	20.2	37.29	15.40	1.226
			40	37.60	18.42	38.56	15.55	1.236

$$S_p = \frac{c_j l_p + N_p \tan \varphi_j}{K}$$

(29)

From Eqs. (24), (26), and (29), the residual thrust of block p is given by:

$$D_p = D_{p-1} + W_p \left(\sin \alpha - \frac{\cos \alpha \tan \varphi_j}{K} \right) - \frac{c_j l_p}{K}$$

(30)

From Eqs. (22), (28), and (30), the residual thrust of the sliding mass is given by:

Under the development of dumping to the coal pillar side or top, the residual thrust of the sliding mass can be written as follows:

$$D_n = D_{n-1} + \left[A_{nm}\gamma_m + (A_n - A_{nm})\gamma_p \right] \left(\sin \alpha - \frac{\cos \alpha \tan \varphi_d}{K} \right) - \frac{c_d l_r}{K}$$

By adjusting the reduction coefficient K so that $D_n = 0$,

(32)

the stability of the inner dump under the sliding surface position can be calculated. Then, by adjusting the position of the

$$\begin{cases} D_2 = W_2 \sin \delta_2 + D_1 \cos(\delta_1 - \delta_2) - \frac{c_2 l_2 + \left[W_2 \cos \delta_2 + D_1 \sin(\delta_1 - \delta_2) \right] \tan \varphi_2}{F} \\ \cdots \\ D_k = W_k \sin \delta_k + D_{k-1} \cos(\delta_{k-1} - \delta_k) - \frac{c_k l_k + \left[W_k \cos \delta_k + D_{k-1} \sin(\delta_{k-1} - \delta_k) \right] \tan \varphi_3}{F} \\ \cdots \\ D_{k+q} = D_{k+q-1} + W_{k+q} \left(\sin \alpha - \frac{\cos \alpha \tan \varphi_j}{F} \right) - \frac{c_j l_{k+q}}{F} \\ \cdots \\ D_{k+q+j} = D_{k+q+u-1} + \left[A_{(k+q+u)m}\gamma_m + \left(A_{(k+q+u)} - A_{(k+q+u)m} \right)\gamma_p \right] \left(\sin \alpha - \frac{\cos \alpha \tan \varphi_d}{F} \right) - \frac{c_d l_r}{F} \\ \cdots \\ D_n = D_{n-1} + W_n \left(\sin \alpha - \frac{\cos \alpha \tan \varphi_j}{F} \right) - \frac{c_j l_n}{F} \end{cases}$$

(31)
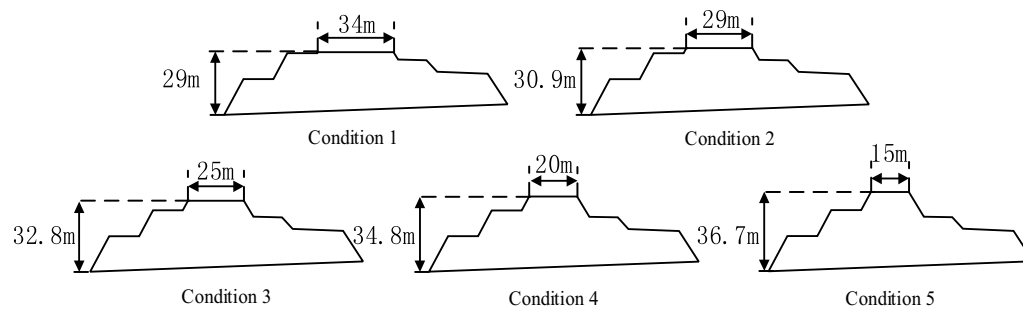
Fig. 12 Cross-sections of the optimal coal pillar shapes under five working conditions

Table 5 Calculation of coal pillar volume

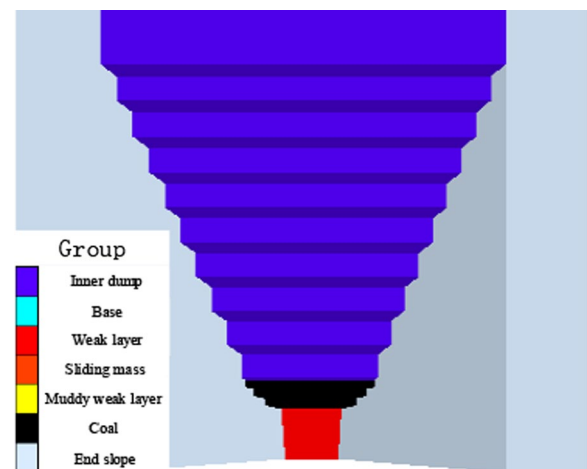| Working condition	b_{best} (m)	h (m)	V (10^4 m^3)
1	34	29.0	29.51
2	29	30.9	29.36
3	25	32.8	29.41
4	20	34.8	28.99
5	15	36.7	28.40

Fig. 13 Numerical simulation model

sliding surface, K can be readjusted to make $D_n = 0$. K_{min} is the stability coefficient corresponding to the most dangerous sliding surface, and is also the stability coefficient F_s of the inner dump. When calculating the overall stability coefficient of the slope, the top width of the section is generally set to twice the height of the slope.

5 Engineering applications

Shengli East No. 2 open-pit coal mine has a design production capacity of 30 million t/a and an economical and reasonable strip ratio of 6 m^3/t. To maximize the mining resources, the coal pillar is mined using the single-bucket-truck process, with a step flat plate width of 15 m, a step height of 12 m, and a step slope angle of 60°. The inner dumping operation is also based on the single-bucket-truck process. The inner dumping yard has a flat plate width of 50 m, a slope angle of 33°, and a step height of 15 m.

To shorten the transportation distance, thus reducing the transportation costs and increasing the economic benefits of the mine, Shengli East No. 2 open-pit coal mine is advancing westward, during which time the inner dump is being developed. As the southern slope is in a creeping state, some of the discharged materials are placed on the roof of the coal seam to avoid large-scale landslides. The inclination angle of the basement of the inner dump is 2°, the lithology of the basement is mainly mudstone, such as kaolinite and montmorillonite, and the primary characteristic is serious softening with water. Waste mainly comes from quaternary clay, tertiary glutenite, mudstone of clay, and coal-measure strata, which have the characteristics of a loose structure and low strength. The typical engineering geology of the inner dump is shown in Fig. 10. According to previous rock test results and slope stability research, the geotechnical physical mechanics indices are presented in Table 1.

## 5.1 Factors affecting slope stability of inner dump

(1) Sensitivity analysis of factors affecting the stability of the inner dump.

The sensitivity of the factors affecting the stability of the inner dump was analyzed using an orthogonal test design method. Orthogonal test calculation results of inner dump stability are presented in Table 2 and a range analysis of these orthogonal tests is presented in Table 3.

Table 3 indicates that the degree of influence of various factors on the stability of the inner dump runs in the order $\beta_p > \alpha > d > h > b > \omega > h_p > \beta$.

In summary, for a specific open-pit coal mine, the coal pillar strike length d, slope angle β_p, and dip angle α of the

Fig. 14 Distribution of displacement and plastic zone

(a) Condition 1

(b) Condition 2

(c) Condition 3

(d) Condition 4
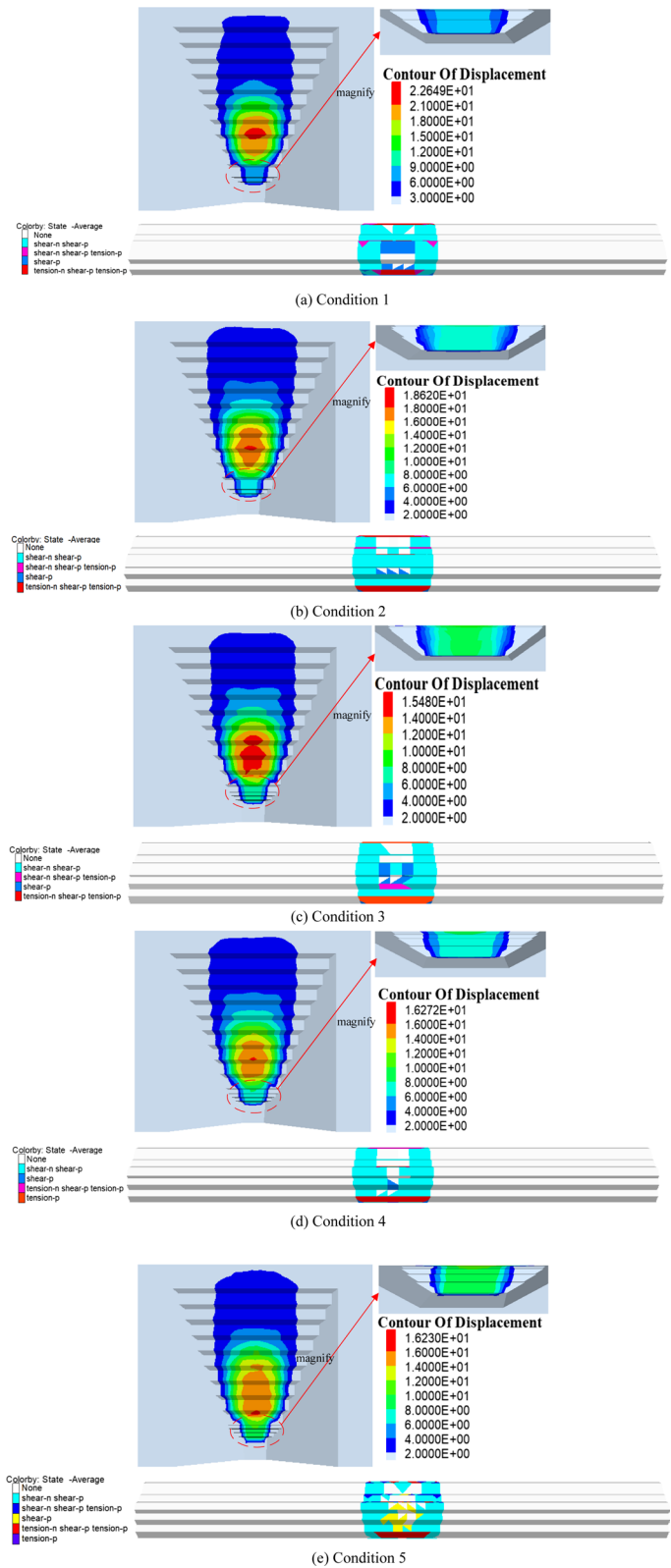
(e) Condition 5

Table 6 Stability calculation result of inner dump

Working condition	Numerical simulation result	Calculation result of this study	Relative error (%)
1	1.22	1.20	1.64
2	1.24	1.20	3.23
3	1.23	1.20	2.44
4	1.24	1.20	3.23
5	1.26	1.20	4.76

base are all fixed values. When a coal pillar is used to support the inner dump, the height h and top width b are prioritized in the optimization of the coal pillar shape parameters, and the outer bottom angle β and inner bottom angle ω are adjusted to satisfy the engineering operation. Thus, only the height h and top width b of the coal pillar should be optimized among the supporting coal pillar shape parameters of the inner dump in Shengli East No. 2 open-pit coal mine.

(2) Influence of various factors on the stability of the inner dump.

We now quantitatively describe the functional relationship between the stability of the inner dump and the various factors, based on the mechanical parameters of the rock and soil mass, and the slope shape of the end slope in Shengli East No. 2 open-pit coal mine. Through Eqs. (14) and (15), the numerical value of the coal pillar supporting effect was calculated using MATLAB. The relationships between the stability of the inner dump and the various factors were fitted using Eq. (31) and the Origin software. The results are shown in Fig. 11.

The results reveal that the slope stability coefficient has a linear relation with the top width and height of the coal pillar, the slope angle, and the base inclination angle. It has an exponential relation with the coal pillar strike length and the slope height increment. The coefficient has a quadratic relation with the coal pillar outer and an absolute value relation with the inner bottom angle.

5.2 Optimization of morphological parameters of supporting coal pillar in the inner dump

Based on the stratum occurrence information and the present situation of stripping engineering, it is known that the inclination angle α is 2° and the coal pillar strike length d is 108 m. To meet the requirements of stripping engineering operations, 15-m-wide transportation flats must be set at the +816 m and +804 m levels. The slope angle of the steps is 65°, and the width of the flat of the inner dump is 50 m;

The slope angle of the step is 33°, the height of the step is 15 m, and the slope angle of the inner dump is about 12°. Under the above conditions and for a typical engineering geological section, when h and b are given, ω, β, d, α, and h_p can be determined. Therefore, the unknown parameters of the shape of the coal pillar in Shengli East No. 2 open-pit coal mine are the height h and top width b. We designed five working conditions, with the minimum coal pillar volume as the criterion, and determined the optimal shape parameters of the coal pillar in the inner dump of Shengli East No. 2 open-pit coal mine. The calculation parameters and results under various working conditions are presented in Table 4, and the resulting coal pillar volumes under each condition are listed in Table 5.

It can be seen from Table 4 that, when the shear resistance T of the side interface of the supporting coal pillar is considered, the minimum value of the equivalent cohesion is 27 kPa and the maximum value is 38.56 kPa. The minimum equivalent internal friction angle is 13.68° and the maximum value is 15.55°. If the shear resistance T of the side interface of the supporting coal pillar is neglected, the cohesion of the bottom interface is 10 kPa and the internal friction angle is 10°. Thus, the cohesion and the internal friction angle increase by at least 170% and 36.8%, respectively, when T is considered. Therefore, the shear resistance of the side interface of the supporting coal pillar cannot be ignored, and the three-dimensional supporting effect of the coal pillar should be considered in the process of coal pillar shape design to avoid any waste of resources.

Analysis of Table 5 shows that the top width of the coal pillar in the inner dump of Shengli East No. 2 open-pit coal mine should be at the level of +824 m. This gives the optimum size of the coal pillar, with a top width of 15 m and a height of 36.7 m.

5.3 Numerical simulation of instability mechanism of the coal pillar and stability of inner dump

To verify the rationality of the instability mechanism of the supporting coal pillar and the stability of the inner dump obtained from the theoretical analysis, the FLAC3D software, which is based on the fast Lagrangian method, was used for analysis (Chatra and Ma 2019; Hamed et al. 2020; Ravi et al. 2017). Considering the applicability of ANSYS for building numerical models and meshing complex engineering-geological bodies and the powerful functions of FLAC3D for geotechnical engineering, the two packages were combined to perform the numerical simulations. The numerical calculations are based on strength reduction theory. The fast Lagrangian finite difference method was used

to solve the slope stability coefficient and obtain the slope instability characteristics. The numerical model was meshed using tetrahedrons with a mesh size of 40 m. Numerical simulations were performed to determine the optimal coal pillar shape parameters and slope shape parameters under the five working conditions when considering the shear resistance of the side interface of the supporting coal pillar. The cross-sectional shapes of the supporting coal pillars for each working condition are shown in Fig. 12, and the numerical simulation results are shown in Fig. 13.

Following several previous studies (Saxena et al. 2019; Wang et al. 2020; Singh et al. 2020; Makowski et al. 2020), suitable boundary conditions were imposed on the numerical model. The boundary conditions for the five working conditions are to impose displacement constraints on the $x = 0$, $x = 950$, $z = 0$, $y = 0$, and $y = 1100$ planes.

(1) Instability mechanism of supporting coal pillar.

It can be seen from Fig. 14 that the displacement of the inner dump slope is relatively small, the displacement of the supporting coal pillar is slightly greater, and the displacement from the fourth flat plate ($+ 905$ m level) from the top to the local slope of the supporting coal pillar is relatively large. Based on the relative stability analysis theory of the slope, the stability of the entire lower part of the inner dump is relatively good, whereas the stability of the central part of the slope is poor. Taking the densest displacement increment contour as the critical sliding surface, the supporting coal pillar fails vertically above the intersection of the end edge and the bottom interface of the supporting coal pillar. It can be seen from the distribution of the plastic zone that, when the supporting coal pillar becomes unstable, the plastic zone mainly suffers from shear failure, local tensile failure occurs, and the shear failure penetrates the entire supporting coal pillar. Therefore, the mechanism of supporting coal pillar instability is a shear failure.

(2) Stability of inner dump.

Taking the horizontal displacement mutation point of the top of the slope surface as the slope instability criterion, the stability calculation results of the inner dump are presented in Table 6.

It can be seen from Table 6 that, under the five working conditions, the stability coefficient of the inner dump calculated by the two-dimensional calculation method is generally lower than that from the numerical simulations. One possible reason for this phenomenon is that the research method used in this study ignores the influence of the end slope on the stress distribution of the supporting coal pillar. Analysis of the relative error shows that the maximum relative error of the two methods is 4.76%, which verifies the rationality of the proposed method for calculating the slope stability of the inner dump considering the development position of dumping.

6 Conclusions

Supporting the coal pillar is an essential component of improving the inner dump stability. This paper has proposed a novel and effective method for ensuring the slope stability of the inner dump under the effect of coal pillar support. Taking an open-pit coal mine as the engineering background, the influence of factors such as the supporting coal pillar shape parameters on the stability was discussed. For a specific open-pit coal mine, the coal pillar strike length, slope angle, and base inclination angle are all fixed; the height and top width of the coal pillar are then prioritized in the shape parameter optimization. The slope stability coefficient has a linear relation with the coal pillar's top width and height, the slope angle, and the base inclination angle, and has an exponential relation with the coal pillar strike length and the slope height increment. Quadratic and absolute value relations have been established with the coal pillar outer and inner bottom angle, respectively. The top width of the coal pillar in the inner dump of Shengli East No. 2 open-pit coal mine should be at the level of $+ 824$ m, and the optimum size of the coal pillar is with a top width of 15 m and a height of 36.7 m. The instability mechanism of the supporting and retaining coal pillar obtained through numerical simulations and the inner dump's stability are in good agreement with the theoretical analysis results. The results presented in this paper provide a theoretical basis for the design, treatment, and safety implementation of similar open-pit mine slope engineering.

Declarations

Competing interest They authors declare that they have no competing interest.

References

Cai MF, He MC, Liu DY (2013) Rock mechanics and engineering. Science Press, Beijing

Chatra D, Ma J (2019) Numerical modelling of rainfall effects on the stability of soil slopes. Int J Geotech Eng 13(5):425–437

Feng SJ, Sun SG, Zhao XF (2014) Research and application of slope stability analysis method based on engineering mechanics and engineering materials. Adv Mater Res 886:432–435

Hamed J (2020) On the behaviour of shallow foundations constructed on reinforced soil slope-a numerical analysis. Int J Geotech Eng 14(2):188–195

Ji YS (2013) Research on instability mechanism and stability control technology of loess base dumping site. Northeastern University, Shenyang

Liu HD, Li DD, Wang ZF (2020) Physical modeling on failure mechanism of locked-segment landslides triggered by heavy precipitation. Landslides 17(2):81–96

Lu N, Han M, Yu L (2019) Stability analysis and optimization of a dump in a mine in Inner Mongolia. Coal Mine Saf 50(09):236–239

Makowski P, Niedbalski Z, Balarabe T (2020) A statistical analysis of geomechanical data and its effect on rock mass numerical modeling: a case study. Int J Coal Sci Technol 4:1–12

Naeini SA, Rabe BK (2012) Bearing capacity and settlement of strip footing on geosynthetic reinforced clayey slopes. J Central South Univ 19(04):1116–1124

Ram GS, Tiwari GN (2019) Simulation performance of single slope solar still by using iteration method for convective heat transfer coefficient. Groundw Sustain Dev 5(10):18–38

Ravi KU, Rajesh S (2017) Soil slope instability along a strategic road corridor in Meghalaya, north-eastern India. Arab J Geosci 10(12):3–9

Saxena N, Saxena A, Mandal A (2019) Synthesis, characterization and enhanced oil recovery potential analysis through simulation of a natural anionic surfactant. J Mol Liq 282:545–556

Shao Q, Wei MC (1998) Soil Mechanics and Basic Engineering. Chongqing University Press, Chongqing

Singh A, Jindal R, Saxena A (2020) Simulation and determination of optimal variables for increased oil recovery potential of surfactant polymer flooding. Offshore Technology Conference Asia.

Tang WL, Peng HG, Ma L (2016) Study on cause and control measures of internal waste dump landslide in open-pit. Coal Technol 35(08):166–168

Tian H (2019) Study on instability law of soft rock slope in Zhundong open-pit mine and safety control technology of high inner dump slope. China University of Mining and Technology, Xuzhou

Wang D, Li GH, Cao LZ, Bai RC, Song ZL (2019) Mechanical effect of supporting and retaining coal pillar on internal waste dump with weak basement. J China Coal Soc 44(03):934–941

Wang JJ, Xiao LL, Zhang J, Zhu YB (2020) Deformation characteristics and failure mechanisms of a rainfall-induced complex landslide in Wanzhou County, Three Gorges Reservoir. China Landslides 17(2):56–76

Wei YF, Nei DX (2013) Analysis on progressive slipping-shear failure mode of bedding slope of hard rock with medium or large dip angle. Appl Mech Mater 438–439:1232–1237

Yang Q, Yin T, Kou HT et al (2018) (2018) Research on the stability of internal dumping site at Baorixile open-cast coal mine. Energy Conserv 02:46–60

Yuan W, Liu SG, Wang W (2019) Numerical study on the fracturing mechanism of shock wave interactions between two adjacent blast holes in deep rock blasting. Earthq Eng Eng Vib 18(04):735–746

Zhang JP, Wang J (2015) Application of energy method in the treatment of weak basement dumps. Coal Technol 34(06):204–205

Zhou XP, Zhu BZ, Juang CH (2019) A stability analysis of a layered-soil slope based on random field. Bull Eng Geol Environ 78(4):2611–2625